

Kpxgunki cvkqp"qp"O wnr ng'T gi ko g'Uj khv"cpf " Gctn{ "Y ctpkpi "F gvgevqp"kp"Eqwr ngf "Uqekq/ Geqmi kecn'P gwy qtm

Hendrik Santoso Sugiarto^{1,2}, Lock Yue Chew^{1,2}, Ning Ning Chung³ and Choy Heng Lai³

¹Division of Physics and Applied Physics, Nanyang Technological University, Singapore 637371

²Complexity Institute, Nanyang Technological University, Singapore 637723

³Department of Physics, National University of Singapore, Singapore 117551

Abstract - The interaction between social and ecological system has become more common nowadays. Complex coupling between these systems can create multiple stable states which possess the danger of a collapse in social cooperation and resources availability. In this paper, we investigate the effects of social network properties on the stability of the system. The modification of hysteresis structure of the system as we vary the social network properties signifies the intimate relationship between the underlying connection of social interaction and the stability of the coupled socio-ecological system. In particular, we want to highlight the characteristic of multiple regime shifts which exist in social network with certain community structures. This characteristic indicates the strength of local collective effects in preventing a collapse of cooperation within the community. Moreover, we have also explored into the accuracies of both temporal and spatial indicators in the detection of early warning signals prior to the impending regime shift. Our results have demonstrated that spatial indicators are more accurate and robust than temporal indicators for early warning detection with respect to changes that arise in the connectivity of social interaction.

1. Introduction

In recent years, the interaction between humans and their environment has become intense and inevitable. Our future is threatened by the prospect of resource scarcity¹ and massive climate change^{2,3}, with humans being the source of the significant deterioration of waters and its hydrologies⁴, forests⁵, as well as biodiversity⁶. Several observations in coupled socio-ecological system (SES) indicate that humans not only act as an external factor, they can also adjust their behaviour in response to ecological alteration^{7,8}. Our ecosystem has experienced sudden, abrupt collapse and long lasting alteration to its structure. Human activities such as industrialization and exploitation are responsible for such collapse of ecosystems⁹. This occurrence is known in the literature as regime shifts. Regime shifts imply the existence of multiple stable states within the system^{10,11}. It happens when gradual alteration of underlying parameters triggers an unexpected transition near a critical point from one stable regime to a new stable regime¹². Multiple stable states also indicate that the state of the system depends not merely on its variables and parameters but also on the history of the system. This path dependency is known as hysteresis, which usually arises via a change of certain driving parameter. Note that such a system cannot be

reversed to its original domain by merely returning the parameter to its previous value. This property of irreversibility within hysteresis makes regime shift catastrophic, in the sense that one cannot return the situation back to its normal state by a simple retraction¹⁰.

In the case of socio-ecological regime shift, catastrophic transition can happen from a failure of cooperation. In real social interactions, the dynamics of cooperation is closely associated with the structure of social interaction. Thus, network properties will affect the local interaction among individuals which affect the multiple stabilities in the system. This in turn affects the bifurcation characteristics and the position of the tipping points of the system. Previous research has connected the relation between network properties and critical transition since the connectivity of network structure is usually associated with a resistance to change which impacts the critical transition between regimes¹³. Therefore, we intend to understand the robustness of different kinds of networks, for instance, what kind of topology would cause the overall systems response to be gradual or catastrophic. This knowledge would give us insights into specific social structures that are less vulnerable to collapse or exhibit the effects of hysteresis. In the context of social network, a vertex corresponds to an individual whereas the edges represent the social interactions. Many model employs an underlying network structure to depict social interactions to improve the reality of their system¹⁴⁻¹⁷. In real life scenario, social network structure often differs from one society to another. Some society also exhibit community structure in which individuals often interact closely within their own community^{18,19}.

With the presence of risk in the sudden and persistent collapse of socio-ecological system, it will be very useful if we are able to anticipate regime shifts before the transition occurs^{13,20,21}. For complex systems, a lack of detailed information makes it difficult to determine the exact position of the tipping point. To circumvent this difficulty, there is a rapid growth in the study of early warning signals of critical transition based on the generic behaviour in the vicinity of regime shifts²²⁻²⁹. Early warning signals can be used as an indicator of a pending regime shift. It gives us enough lead time to pre-empt the regime shift or to start

evacuation procedure if the regime shift is unavoidable^{13,30}. However, early warning signals cannot predict the future transition accurately all the time³¹⁻³³. There are possibility of false positive (when the early warning signal indicates an approaching transition but turns out to be false detection) and false negative (when the early warning signal failed to predict the approaching transition). In this paper, we will explore the applicability of conventional early warning signals such as autocorrelation and standard deviation to detect the occurrence of regime shifts accurately.

2. Model

A specific example of a simple coupled socio-ecological model is the Common Pool Dilemma. This problem is interestingly described by Hardin as a tragedy of the commons³⁴. In this problem, the maintenance of the ecological resource requires cooperative behaviour among related individuals who have equal access to the common resource. The collapse of cooperation is inevitable if everyone is rational and selfish since every selfish act to maximize individual profits will lead to a depletion of resources which in turn destroys the economic viability of the whole system. Common pool dilemma is very relevant to our situation today because the increasing competition for the common ecological resources is the main culprit that damages our natural ecosystem.

In this system, the natural component can no longer be treated merely as a resource reservoir. It can also be considered as a production factor which directly affects the actual production yields³⁵. In many common pool models, production is described by using the Cobb-Douglas function with decreasing returns, i.e. $F = \gamma E^\alpha R^\beta$, where E is the total effort and R the resource available³⁶⁻³⁸. The value of the constants α, β, γ affects the shape of this function. Since the production function has the feature of decreasing returns, we expect $\alpha + \beta < 1$. Note that we use $\alpha = 0.6$, $\beta = 0.2$, $\gamma = 10$ in our simulation. The total payoff is then described by subtracting the opportunity cost from the production function: $\pi_c = \frac{e_c}{E} F - we_c$ for co-operator, and $\pi_d = \frac{e_d}{E} F - we_d$ for defector, where $w = 15$. Previously, Tavoni et al proposed an ostracism mechanism to maintain the cooperation among resource users³⁸. This model is called the TSL model, which is formulated in the form of non-linear dynamical equations consisting of two main components: the social dynamics and the ecological dynamics. In this paper we retain all important features of the TSL model. TSL model employs an equity driven ostracism mechanism to maintain the cooperation level, which leads to the following utility: $U_d(n_c) = \pi_d - O(n_c) \frac{\pi_d - \pi_c}{\pi_d}$ for defector and $U_c = \pi_c$ for co-operator. $O(n_c) = he^{tegn_c}$ is the ostracism function with the parameter $h = 0.34$ representing the ostracism strength, and the parameters $t = -150$ and $g = -10$ govern the shape and effective threshold of the ostracism function. The rate of change of the available ecological resource is made up of

3 components: linear resource inflow, natural depreciation and human extraction: $\frac{\Delta R}{\Delta t} = c - d \left[\frac{R}{R_{max}} \right]^2 - ER$. where, $d = 50, R_{max} = 200$

The central assumption of previous model is a well-mixed social interaction, which makes the ostracism mechanism effective against defectors. To make it more realistic, we have modified the model by adding social network to constraint social interaction among users. We have also incorporated discrete updating so that the social and ecological variables are evaluated at every time step. The schematic image of this model is shown in figure 1a below.

In this paper, all individuals interact locally with their adjacent neighbours in a specific social network. The social interaction here involves ostracism as social sanction with utility comparison. Moreover, we shall consider social interaction based on the Erdos-Renyi network topology, scale-free network topology, and also network with community structure. For the updating mechanism, we use asynchronous pairwise comparison such that at each time step a random player updates his strategy after comparing his utility against his random neighbour. This mechanism is usually called strategy selection and its details are shown in figure 1b. If the utility of his matched neighbour is higher than his utility, he will adopt his neighbour's strategy with a certain probability which is proportional to the utility difference between him and his matched neighbour. Beside strategy selection, we also include the mechanism of mutation where we flip the strategy of a randomly chosen individual after a certain period of time (see figure 1c). The mutation mechanism is necessary to avoid the system being trapped in the state of all agents adopting the same strategy.

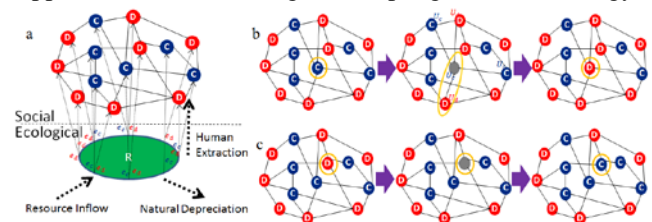


Figure 1. Model. (a) Our model consists of both a social and an ecological system. The resource within the ecological system is increased through a linear resource inflow, and decreased via natural depreciation and human extraction. Each individual within the social system interacts based on a social network topology. Their payoffs depend on their ecological resource extraction. If the individual is a defector, an additional cost due to ostracism through social interaction with its neighbours has to be subtracted from his utility. A co-operator (blue) agrees to extract less resource according to the prior agreement and ostracizes any defectors that are connected to them. On the other hand, a defector (red) maximizes its payoff by extracting more than the agreement. The updating mechanism in (b) represents the process of selection. At each time step, a random individual compares his utility with that of a random neighbour. The probability of an individual changing his strategy to the opposite strategy is proportional to the utility difference. The updating mechanism in (c) represents the process of random mutation. At a certain mutation period, a random

individual is selected to reverse its strategy (from co-operator to defector, or vice versa).

3. Methods

In this section we proceed to introduce the methods we employ to analyse our model. The analysis shall consist of two parts: the phenomenon of hysteresis with the presence of multiple stable states, and the early warning signals of the upcoming regime shifts. The coupling between the social and ecological aspects of the system creates a strong correlation between the fraction of co-operators and the availability of resources, which lead to similar results for these two components. In consequence, we shall only focus on the social component of the system and drop the ecological part in our discussion.

3.1. Hysteresis and Multiple Stable States

Our system can fall into either a cooperative or a defective regime. In order to obtain a good approximation of the hysteresis cycle with multiple stable states, we average our results over many cycles. Note that a single cycle is defined as moving the socio-ecological states once around the hysteresis loop by adjusting the control parameter. For our studies, initial conditions are chosen such that the system begins at the cooperative regime. To ensure that the system is in the steady state, we evolve the system for a sufficiently long time before altering the value of our control parameter. For the first half of a hysteresis cycle, we increase the control parameter continuously and quasi-statically, driving the system gradually along the steady state values within a particular regime. The new state is then recorded when a new equilibrium is reached after each alteration. This process is repeated until a critical parameter is exceeded and the system undergoes a regime shift. We then reverse the process to evolve the system towards its initial state. Note that each complete cycle of parameter alteration gives a hysteresis curve.

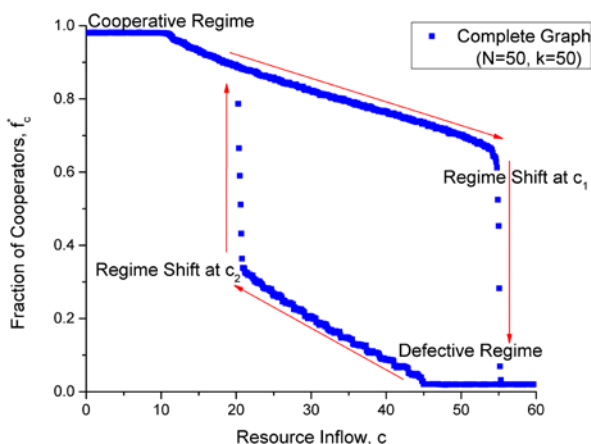


Figure 2. Hysteresis Structure. The blue square symbol represents the average over 100 cycles of fraction of co-operators at equilibrium for different resource inflow c . The simulation starts at $c=0$ and stops at $c=60$. The system is evolved at a fixed c for a sufficiently long time in order for the state to reach its equilibrium value. The parameter c is then increased by 0.1 and the process is

repeated. After we have completed the computation of all equilibrium points between $c=0$ and $c=60$, we reverse the process and determine the equilibrium points by varying c from 60 to 0. This whole process represents a single cycle of hysteresis. It is repeated and averaged over 100 cycles to produce the above average hysteresis cycle.

Figure 2 shows the hysteresis curve of a system based on social interactions from a complete graph of 50 individuals driven by a variation in the amount of resource inflow as our control parameter. Note that various control parameters whose adjustment can lead to the hysteresis cycle, but for simplicity, we shall only concern with resource inflow as our control parameter in this paper. The result in Fig. 2 was averaged over 100 simulations. As the system becomes close to the first transition point c_1 , a further increase in the amount of resource triggers a critical transition towards the defector equilibrium. Once the transition takes place, the previous states of the system cannot be restored through reversing the same path. During the second half of the hysteresis cycle, the cooperativeness of the population does not increase sharply back to its previous values at c_1 as we decrease the amount of resource inflow. Instead, it increases slowly by tracing a distinct path before a second transition point c_2 is reached. Then, a further reduction in the amount of resource inflow triggers another sharp transition: from the defective regime to the cooperative regime.

3.2. The Analysis of Early Warning Signals

Typically, early warning signals are obtained by exploiting the generic behaviour of the system close to critical transition, such as the phenomenon of critical slowing down. However, these early warning signals normally suffer from false detection. Previous research has provided a statistical comparison between the results from the test model and the null model to determine the accuracy of the model^{32,33,39}. One of them is Receiver-Operating Characteristic (ROC) which is a very robust method for the evaluation of the performance of various indicators and to capture their trade-off between both false positive and false negative qualitatively³³. However in this paper, in order to obtain the accuracy quantitatively, we compare the probability distribution of test model and null model directly by using p-value significant testing.

The test model relates to the case where our control parameter increases very slowly till it reaches the tipping point (10 increments in 10,000 steps), i.e. we select the portion that precedes the potential transition. On the other hand, the null model is the situation without regime shift where the control parameter is kept fix, such that the system is only driven by stochastic fluctuations. The network that we use to test the accuracy of our early warning signal detection approaches is the Erdos-Renyi network. We have used a population size of $N=50$ and various average network degree in our investigation. The early warning signals can be obtained by means of either temporal patterns or spatial

patterns. The accuracy of the early warning signals for different network degrees will be compared and discussed.

3.2.1. Temporal Patterns

Temporal early warning signal is often handy because in most cases the time series data is the only information available to us. The data analysis that yields the early warning signals of interest usually requires several steps which include pre-processing, filtering, probing, and significance testing whose details can be found in Dakos et al.²². In empirical observations, we are typically restrained by the frequency of observation (i.e. the time interval between points in the datasets). However, this does not happen in our case since our time series data arise from the model, and our results show that the accuracy of the early warning signals obtained is independent of the frequency of observation. Therefore, we only illustrate situations when the time interval is 50. In this analysis, we use a rolling window with a size that is half of the whole time series datasets. We also filter the trends by using Gaussian smoothing to avoid spurious indications caused by the presence of strong local correlation structures in the time series (figure 3a, panel 1). The de-trended data (figure 3a, panel 2) is then analysed by several conventional indicators such as autocorrelation, standard deviation, skewness and kurtosis. We have quantified the indicator's trends by using the Kendall tau rank correlation which was computed through the R package: 'early warnings' (figure 3a, panel 3-6). To achieve the statistical comparison, we have replicated 1,000 realizations for each time series measurement from our simulation for both the case of test model and the null model. The distributions for both cases are compared to determine the accuracy of the early warning indicators (figure 3b, panel 1-4). Note that the vertical lines indicate the p value = 0.05 of the null model. Any value beyond these lines is considered significant. The accuracy of specific indicator is then quantified by the proportion of significant predictions attained against the total number of predictions attempted.

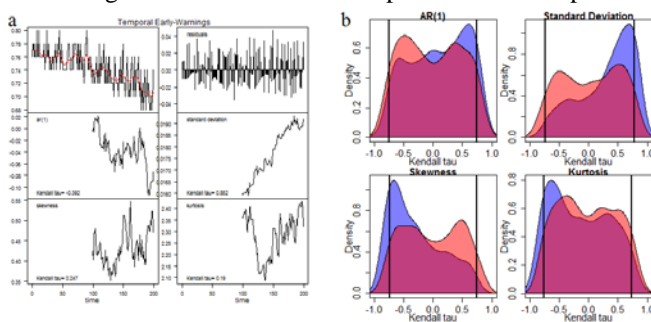


Figure 3. Procedure for temporal early warning signals. Figure (a) represents a single realization of early warning detection. Panel 1 gives the time series of the fraction of co-operators. The red curve is obtained after passing the time series through a Gaussian filter. Panel 2 shows the de-trended data that is employed for subsequent analysis. Each indicator is calculated within a rolling window that is half the size of the whole data. Panel 3-6 illustrates the trend for the following indicators: autocorrelation at lag-1, standard deviation, skewness, and kurtosis. The trend is then

further analysed by means of the Kendall tau rank correlation. Figure (b) shows a comparison between the null model and the test model for each temporal indicator. The distribution in red represents the trend from the 1000 realizations of the null model. The vertical lines indicate the positions of the p-value = 0.05. On the other hand, the blue distribution represents the trend from the 1000 realizations of the test model.

3.2.2. Spatial Patterns

Spatial early warning signal is only useful if we have complete spatial information of the system. It often provides more accurate predictions in comparison to temporal early warning signal, although it is more difficult to exploit due to insufficient spatial data in many cases. In our work, the spatial pattern is obtained from the spatial distribution of each strategy (cooperative or defective) within the network structure. The spatial autocorrelation is quantified by means of the Moran spatial correlation, $I = \frac{(N \sum_{i=1}^N \sum_{j=1}^N w_{ij} (x_i - \bar{x})(x_j - \bar{x}))}{(\sum_{i=1}^N \sum_{j=1}^N w_{ij}) \sum_{i=1}^N (x_i - \bar{x})^2}$, where $w_{ij} = 1$ if node i and j are adjacent in their network structure, and $w_{ij} = 0$ otherwise. i and j refer to the location of a node which represents an agent within the network structure. In our calculations, we let $x_i = 1$ if agent i is using the cooperative strategy and $x_i = 0$ if agent i is using the defective strategy. The standard deviation, skewness and kurtosis are modified into spatial measures as the second, third, and fourth moments about the spatial mean respectively⁴⁰, i.e. the spatial variance is formally defined as $\sigma^2 = \frac{1}{N} \sum_{i=1}^N (x_i - \bar{x})^2$, the spatial skewness $\gamma = \frac{1}{N} \sum_{i=1}^N \frac{(x_i - \bar{x})^3}{\sigma^3}$, the second moment of spatial mean $\kappa = \frac{1}{N} \sum_{i=1}^N \frac{(x_i - \bar{x})^4}{\sigma^4}$. In many spatial early warning methods, a 2 dimensional space discretized into M and N units in x and y direction has been employed^{25,40}. However, since the spatial structure in our paper is defined with respect to the agent's strategy which is organized in terms of network topology, we use the definition of local and global network statistics⁴¹.

Similar to the temporal early warning method, we record the value of each indicators as the system approaches the critical transition. As the system gets closer to critical transition, we expect an increase in spatial autocorrelation and standard deviation. We shall quantify the trends exhibited through the spatial indicators by means of the Kendall tau rank correlation (figure 4a, panel 1-4). In order to achieve statistical comparison we have generated 1,000 realizations from time series simulation for the case of test model and also the null model. The test model is the trend of spatial indicator when the system is approaching critical transition and the null model is the trend of spatial indicator when the system is not approaching critical transition. These are illustrated in panel 1-4 of figure 4a. The distributions obtained for these two cases are then compared to determine its accuracy (figure 4b). Note that the vertical lines indicate the p value = 0.05 of the null model. Any value beyond these lines is considered as significant. Again, the accuracy

of the specific indicator is quantified by the proportion of significant predictions achieved against the total number of predictions attempted.

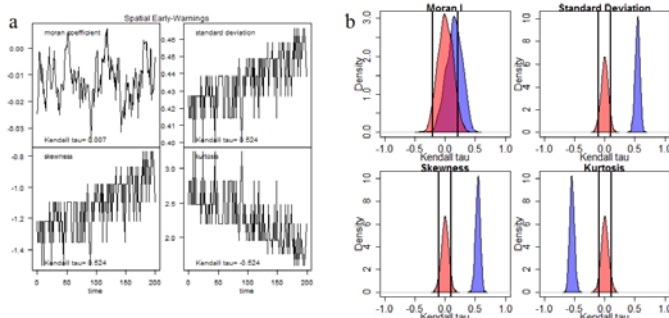


Figure 4. Procedure for spatial early warning signals. Figure (a) illustrates a single realization of spatial early warning signals. Panel 1-4 give the trend of spatial autocorrelation (Moran coefficient), standard deviation, skewness, and kurtosis respectively. The trend is then analysed using the Kendall tau rank correlation. Figure (b) shows a comparison between the null model and the test model for different spatial indicators. The distribution in red is obtained from the trend of 1000 realizations of the null model. The vertical lines show the position of the p -value = 0.05. The blue distribution is derived from the trend of 1000 realizations of the test model.

4. Results

4.1. The Effect of Network Properties on Hysteresis Structure.

In this section, we shall present our numerical results and discuss the effects of several network properties on the hysteresis structure of the system.

4.1.1. Degree

Some societies are more connected than others. Therefore, it is reasonable to study the effects of network degree and investigate its consequences on coupled socio-ecological systems. This has led us to employ the Erdos-Renyi graph with a size of $N=50$ as our social network. We shall vary the average degree (k) of this network to model societies with different average number of social connections. The resulting set of hysteresis structures obtained is presented in Fig. 5. We observe that as the average degree k decreases, the width ($\Delta c = |c_1 - c_2|$) of the hysteresis curve reduces. As shown in Fig. 5, critical transitions happen around $c_1=50$ and $c_2=22$ for a population with $k=45$. When the network has a lower degree (for example $k=25$), the regime shift towards the defective regime happens earlier (at $c_1=40$) while the regime shift towards the cooperative regime occurs at a slightly larger value of resource inflow ($c_2=25$). Interestingly, hysteresis effect is no longer observed for a population with very low number of social connection (i.e. $k=5$). When the number of social ties is small, a reduction or increment of a single co-operator can have a large impact on the effectiveness of social ostracism within the local co-operator communities. In this case, the fraction of co-operators decreases faster as the control parameter increases and the system may regain its original state by following the same path as we reverse

the process. On the other hand, when there are a large number of social connections, the reduction or increment of a single co-operator has relatively less impact on the effectiveness of social ostracism. Hence, there exists a critical point when social sanction can no longer hold the extra payoff offered by defective behaviour.

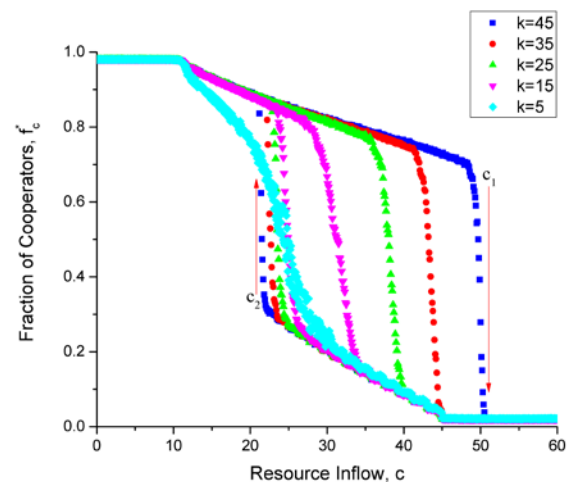


Figure 5. The effects of network degree on hysteresis structure. The simulation is based on the Erdos-Renyi random graph topology with network degrees ranging from $k=45$ to $k=5$ and a population size of $N=50$. We plot the fraction of co-operators versus resource inflow obtained from the simulation results for degree $k=45$ (represented by blue square symbol) to $k=5$ (represented by cyan diamond symbol) at a decrement of 5 unit each (see legend for the different colour and symbol). Note the reduction in hysteresis width as the degree is lowered.

4.1.2. Topology

Most real world social networks are not random graphs. Here, we study the influence of network topologies on regime shifts in coupled socio-ecological system. Specifically, we compare the effects of two different network topologies: the Erdos-Renyi random network, and the scale-free network generated using the Chung-Lu algorithm⁴² on the hysteresis structure. Note that we have raised the population size to $N=200$ in order to enhance the effects from the scale-free network. Simulation results are shown in figure 6, where we noticed a difference in hysteresis width between the two hysteresis curves. Although these networks have the same degree, a scale-free network comprises a greater proportion of nodes with a larger degree. This feature boosts the effectiveness of the ostracism mechanism within the co-operative regime of a society with a scale-free network structures, such that the critical transition is prevented from happening earlier. Furthermore, since the effectiveness of the ostracism mechanism is dependent on the presence of a certain number of co-operators, the degree structure of the network has minimal effect when the state of the system is within the defecting regime. As a result, the critical transition from the defective regime into the cooperative regime occurs at similar control parameter value.

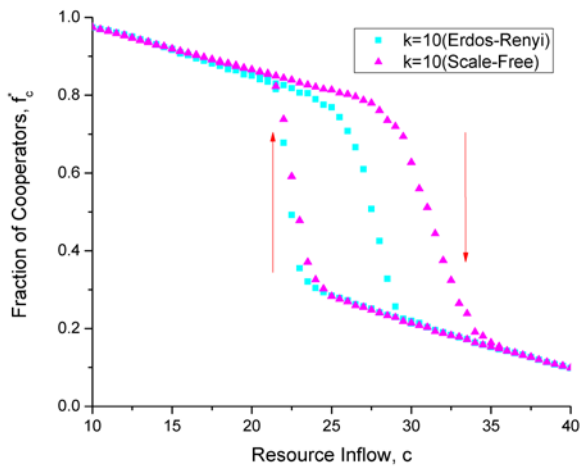


Figure 6. The effects of network topology on hysteresis structure. The cyan square represents the numerical results from the Erdos-Renyi random network topology, while the magenta triangle corresponds to that of a scale free network from the Chung-Lu algorithm. We have increased the population size to $N=200$ in order to capture the scale free effect. Note that we have set the range of the control parameter c from $c=10$ to $c=40$.

4.1.3. Community Structure

In many societies and global organization of the real world, social connection is found to consist of several structural subunits or communities associated with strongly interconnected components¹⁸. To study the effects of such social organizations with sub-structural units, we construct an artificial network with the properties of community structure. The community structure is created by rewiring the original Erdos-Renyi graph via a classification of all the nodes into several community groups. The quantifier “parameter mixing” (μ) measures the fraction of intergroup connections against the total connections within the network, and hence it indicates that each node shares a fraction μ of its links with other community⁴³. In this section, we consider a population size of $N=100$. This choice is motivated by practical considerations since 100 individuals can be easily divided into groups of 2, 4, and 5 with equal number of individuals within each community group. Figure 7 below displays two network structures with 4 community groups each that possess different mixing parameter μ .

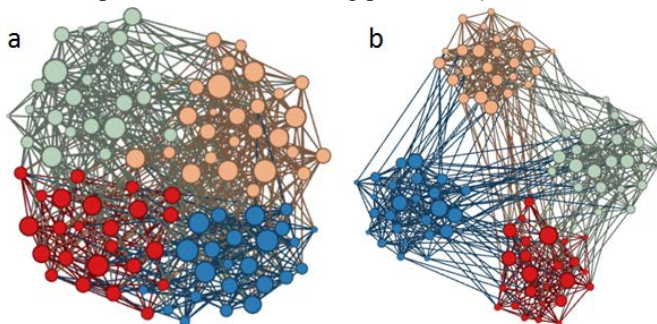


Figure 7. Networks with Community Structure. Both figures illustrate Erdos-Renyi network with an average degree of $k=15$. These networks possess community structures of different mixing parameters. Note that colour is used to differentiate between

different community groups, while node size serves to indicate the number of neighbouring connections. Figure (a) A network with community structure of mixing parameter 0.4; Figure (b) A network with community structure of mixing parameter 0.2.

Our simulation results are shown in figure 8. Here we study the effect of mixing parameter μ on the hysteresis structures. These figures illustrate the case of a network with low degree ($k=5$, figure 8a) and high degree ($k=45$, figure 8b) consisting of 2 community groups. For all cases, we observe that as μ is reduced (modularity is increased), the regime shift tends to occur earlier from the cooperative regime to the defective regime. This effect is more apparent in the case of a higher degree network. Interestingly, we also observe multiple hysteresis in the case of a higher degree network as we reduce the mixing parameter μ . Instead of a total collapse or a total revival, the system is found to collapse or revive in a step by step manner.

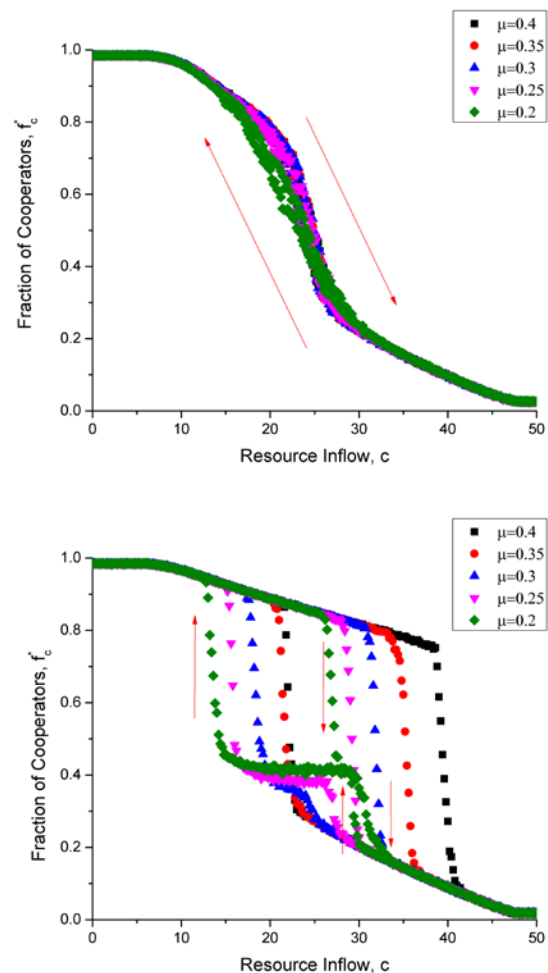


Figure 8. The effects of mixing parameter on the hysteresis curve. The simulation is based on a modified random graph with a topology that contains community structure. Note that the network is fixed with a population size of $N=100$ consisting of 2 community groups. The results are obtained from simulations based on mixing parameters that range from $\mu = 0.4$ (represented by square symbol) to $\mu = 0.2$ (represented by diamond symbol) with a decrement interval of 0.05 (see legend for the different symbols) for (a) a lower network degree ($k=5$); and (b) a higher network degree ($k=45$).

We also observe similar conclusion for any number of community groups. The results are shown in figure 9, where we observe a change in the hysteresis structures as μ varies. These figures illustrate the case of a network with degree $k=15$ consisting of 2 and 4 community groups. Similar to our previous findings, the regime shift tends to occur earlier from the cooperative regime to the defective regime as μ is lowered (or modularity is increased). We expect this effect to occur for any number of community groups although we have only displayed the results for 2 and 4 community groups. In the case when μ is small, the ostracism mechanism operates mainly within the individual community which tends to isolate from each other due to the stronger intra-group connections. Since ostracism is effective only beyond a critical number of co-operators, its applicability as a social mechanism against selfish behaviour reduces as individuals become more isolated within each separate group. In consequence, the shift from the cooperative to the defective regime occurs earlier. Furthermore, for very low μ , we again observe the occurrence of multiple hysteresis where a step by step collapse or revive is observed. From the plot (figure 9b), we observe that the multiple hysteresis and the steps of the regime shifts are obscured due to the averaging effect. In fact, several tipping points of the last few steps have been averaged out and become mixed into a single shift.

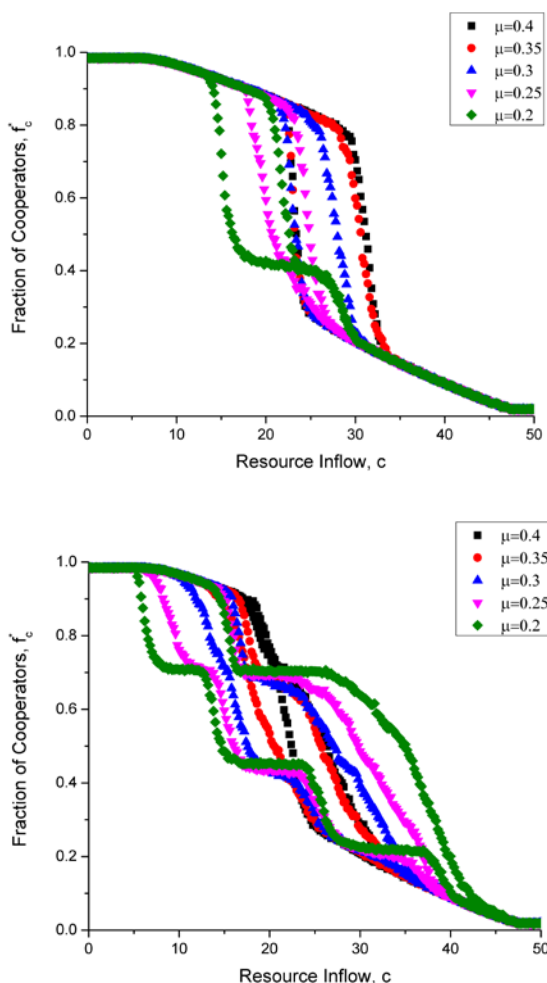


Figure 9. The effects of community structure on the hysteresis curve. The simulation is based on a modified random graph with a topology that contains community structure. Note that the network is fixed with a degree of $k=15$ and a population size of $N=100$. The results are obtained from simulations based on mixing parameters that range from $\mu = 0.4$ (represented by square symbol) to $\mu = 0.2$ (represented by diamond symbol) with a decrement of 0.05 unit (see legend for the different symbols) for (a) 2 community groups; and (b) 4 community groups.

In order to gain a better picture on the reasons behind the multiple hysteresis phenomena, we have plotted single realizations of hysteresis cycle in a network structure with 5 community groups for $\mu = 0.2$. We have plotted the fraction of co-operators within each community as well as that within the whole society. The results show that as the control parameter increases, the cooperative behaviour does not collapse globally but instead locally within the community. More precisely, we can see from figure 10 that the cooperativeness within community 2 collapses first while those of other communities continue to survive. As the control parameter is further increased, community 4 is observed to collapse next. This is followed by community 1 and then community 5. Finally, community 3 collapses. Interestingly, the network community structure prevents the ostracism mechanism to act effectively across communities and thus prevent the concomitant collapse of cooperative behaviour across the whole society. It is interesting that the reversal of the communities from the defector regime to the cooperation regime does not necessarily follow the same sequence as that when the cooperation of the communities collapses. By combining all the hysteresis structures of each community, we then observe the multiple hysteresis of the whole population as represented in bold colour in figure 10.

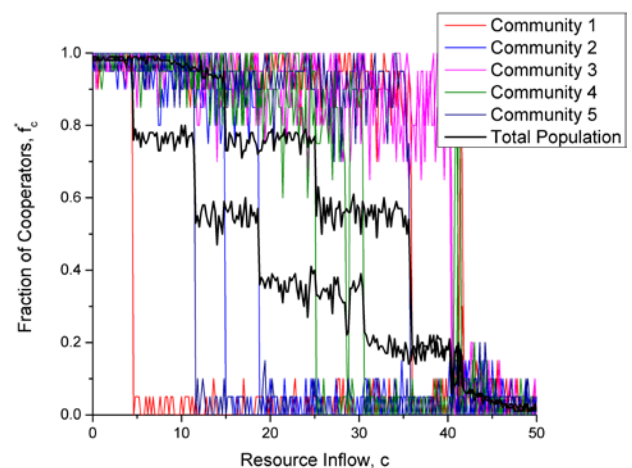


Figure 10. Single realization of the effects of community structure on the hysteresis curve. The simulation is performed according to a modified random graph with the topology of community structure. Note that the network is fixed with a degree of $k=15$, a population size of $N=100$, and a mixing parameter of $\mu = 0.2$. We have plotted the fraction of co-operators against resource inflow for each community which is represented by curves of different colour. The colour in bold is for the case when we consider the whole population.

So far, we have only dealt with community groups of equal size. We might wonder whether the result is robust when each community groups has different population. To explore this, we perform simulation on a network structure with 4 community groups. The size of each community groups are: 10, 20, 30, and 40. Thus, the total population size is 100. We use a mixing parameter $\mu = 0.2$. Similar to our previous simulation, we have plotted the fraction of co-operators within each community as well as that within the whole society (in figure 11 below). Our simulation results again demonstrate the phenomenon of multiple regime shifts. We observe that the magnitude of the collapse of social cooperation depends on which community collapses. For instance, when cooperation within community 4 collapses, the number of cooperative individuals within the total population would have the largest reduction. In the realization within our simulation, we observed that the cooperativeness within community 2 collapses first, followed by 1 and 3, and finally community 4. Community with large population, for instance, community 4 usually collapses last because of stronger internal ostracism mechanism which serves to maintain the internal cooperation. Interestingly community with small population size does not necessarily collapses first, because although their internal ostracism is weaker, individuals in this community are seldom influenced by the opposite strategy due to their small size and low probability to be connected with individuals of different strategies. This suggests that a small community size does not imply a disadvantage situation.

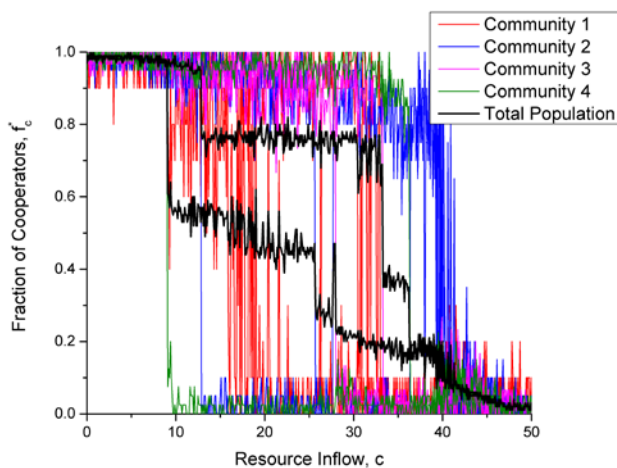


Figure 11. A single realization on the effects of unequal community population size on the hysteresis curve. The simulation is performed according to a modified random graph with the topology of community structure. Note that the network is fixed with a degree of $k=15$, a population size of $N=100$, and a mixing parameter of $\mu = 0.2$. The size of community 1 is 10, community 2 is 20, community 3 is 30, and community 4 is 40. We have plotted the fraction of co-operators against resource inflow for each community which is represented by curves of different colour. The colour in bold is for the case when we consider the whole population.

4.2. Early Warning Signals.

In this section, we shall show our numerical results and discuss the effects of network connectivity on the accuracy of several conventional early warning signals. Note that all the necessary details with regards to the early warning signals have already been discussed in the methods section.

4.2.1. Temporal Patterns

Figure 12 illustrates a comparison of the test model distribution and the null model distribution for the temporal early warning signals. For this, we have recorded all the Kendall tau correlations for each indicator, and plotted them in the form of distribution in order to compare the test and the null model. The indicators are considered accurate when the null and the test distributions are distinguishable. Note that we have used a p -value=0.05 (vertical line) as our standard of comparison. Figure 12a gives a comparison on the distributions for low degree ($k=5$) and figure 12b for high degree ($k=45$). From these results, we observe that only the distributions from the indicator based on standard deviation is distinguishable. Furthermore, if we were to compare the performance of the standard deviation indicator for the case of low and high network degree, we observe that the distributions are easier to be distinguished when the social interactions possess lower connectivity.

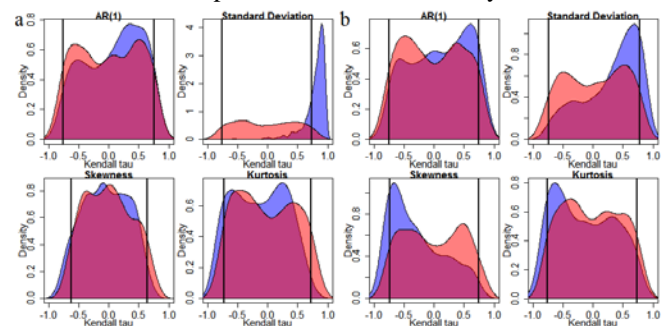


Figure 12. Comparison of the null distribution and test distribution for temporal early warning signals. A plot on the Kendall tau distribution of different temporal early warning indicators: autocorrelation at lag-1, standard deviation, skewness, and kurtosis (see legend), between the null and the test model for (a) low network degree ($k=5$) and (b) high network degree ($k=45$). The distribution in red represents the trend from the 1000 realizations of the null model. The vertical lines indicate the positions of the p -value = 0.05. On the other hand, the blue distribution represents the trend from the 1000 realizations of the test model.

The relation between early warning signals and network connectivity can be seen more clearly in Figure 13. Figure 13 shows the accuracy of specific temporal indicators as the network degree varies. Our results here show the percentage of significant correct prediction. We found that most of the temporal early warning signals are not accurate enough to predict the approaching transition. From the figure, we can see that only temporal standard deviation is sensitive enough to detect future regime shift. Other indicators are not able to distinguish between the null model (stable system) and the test model (system approaching

critical transition). We observe that the accuracy of the temporal standard deviation increases as the network degree is lowered. This results from the following. For the case of high degree network, the stability of the regime reduces gradually as the control parameter increases. On the other hand, the stability drops faster in the case of low degree network as the control parameter increases. Since the dynamics of the system fluctuates more rapidly (higher variance) when the system is unstable, the temporal standard deviation is able to capture the increasing trend of variance more effectively. This explains why the temporal standard deviation performs better when the network degree is low versus that when the network degree is high.

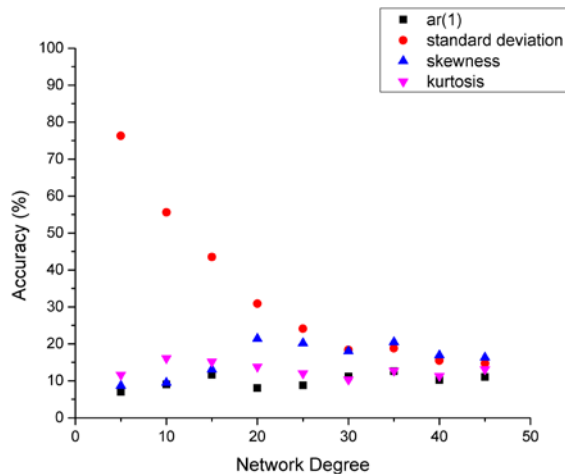


Figure 13. Accuracy of temporal early warning signals. A plot on the accuracy of different temporal early warning indicators: autocorrelation at lag-1, standard deviation, skewness, and kurtosis (see legend), versus the network degree. Note that each point is obtained after determining the percentage of significant accurate predictions through a comparison made against the null model.

4.2.2. Spatial Patterns

Similar to the case of temporal patterns, Figure 14 illustrates a comparison of the test model distribution and the null model distribution from spatial early warning signals. All the Kendall tau correlations for each indicator are recorded and plotted in the form of distribution in order to compare the test model with the null model. The indicators are deemed accurate if it can lead to a substantial spacing between the distribution for the null and the test model. We use a p -value=0.05 (vertical line) as our standard of comparison. Figure 14a gives a comparison on the distributions for the case of low degree ($k=5$) and figure 14b for the case of high degree ($k=45$). From our results, we observe that most of the spatial indicators are effective early warning detectors. Only the indicator based on spatial correlation gives rise to an overlap between the null and the test distribution. Nonetheless, this overlap is observed to disappear in the case of low degree network. Therefore, we can again conclude based on the distinguishability of the null and test distributions that the spatial correlation indicators perform better for social interactions with a lower level of connectivity.

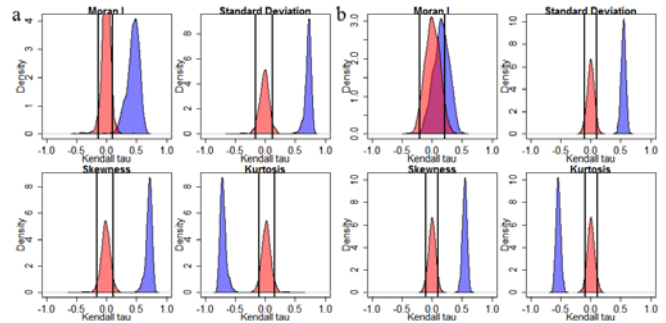


Figure 14. A comparison of the null distribution and the test distribution for spatial early warning signals. A plot on the Kendall tau distribution of different spatial early warning indicators: Moran I spatial correlation, spatial standard deviation, spatial skewness, and spatial kurtosis (see legend), between the null model and the test model for (a) low network degree ($k=5$) and (b) high network degree ($k=45$). The distribution in red represents the trend from the 1000 realizations of the null model. The vertical lines indicate the positions of the p -value = 0.05. On the other hand, the blue distribution represents the trend from the 1000 realizations of the test model.

The relation between early warning signals and network connectivity can be seen more clearly in Figure 15. Figure 15 shows the accuracy of specific spatial indicators (Moran I, standard deviation, skewness, kurtosis) as the network degree changes. In comparison to the temporal early warning signals, we found that most of the spatial indicators are sensitive enough to predict the occurrence of an approaching regime shift. In fact, the second, third, and fourth moment of the spatial mean (i.e. the standard deviation, skewness, and kurtosis) are able to predict the approaching regime shift with 100% accuracy. For these indicators, the distribution of the null model and the test model is found to be totally separated without any overlap. The separation between the test model and the null model indicates the underlying accuracy of the model since the early warning signal can be clearly distinguished from the false signal. Far away from the critical transition, only the strategy of mutation is dominant in the updating mechanism. Therefore, the strategy of each node varies near the spatial mean of the null model, as indicated by the second, third, and fourth spatial moments. On the other hand, since the strategy of selection is dominant in the test model, the strategy of each node is observed to vary far from the spatial mean.

In the case of spatial correlation, the accuracy of the Moran I is found to increase as the network degree is lowered, and it can predict with 100% accuracy when the degree is very low. This can be understood as follow. Near the critical transition, we can perceive that every part of the network becomes spatially more similar to each other. For high degree network, since everyone is almost connected to everyone else, the system is already spatially correlated even for the null model. This makes it difficult to distinguish between the null and the test model. Such spatial correlation reduces as the network degree decreases, thus enabling the null model to be distinguishable from the test model. Spatial

early warning signals are found to be more robust for the detection of approaching regime shift compared to temporal early warning signals. In reality, however, this approach is very difficult to achieve practically because there is a need to have complete spatial strategy information of every individual. Perhaps in the future, it is possible to obtain the spatial behaviour and social network of every individual through big data by means of smart phone location tracking or social networking services.

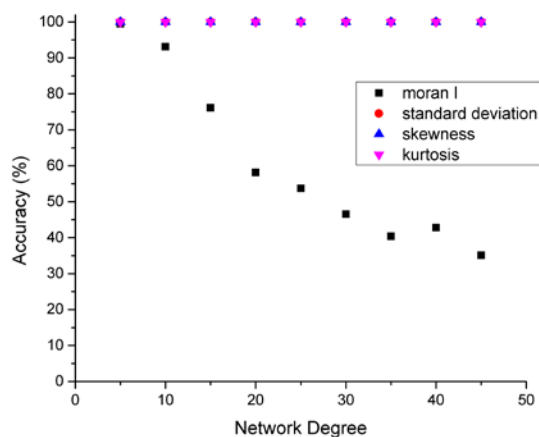


Figure 15. Accuracy of spatial early warning signals. A plot on the accuracy of various spatial early warning indicators: Moran coefficient, spatial standard deviation, spatial skewness, and spatial kurtosis (see legend), versus the network degree. Note that each point is obtained after determining the percentage of significant accurate predictions through a comparison made against the null model.

As we mention before in the methods section, the result is consistent for any frequency of observation (i.e. the time interval between points in the datasets). Figure 16 below represents the accuracy of Moran I spatial correlation indicators with different observation period. The result indicates that the accuracy of the early warning signals obtained is independent of the observation period. Observation period here refers to time interval between two consecutive observations. The measurements for other indicators, be it spatial or temporal indicators, are also found to be independent of the observation period

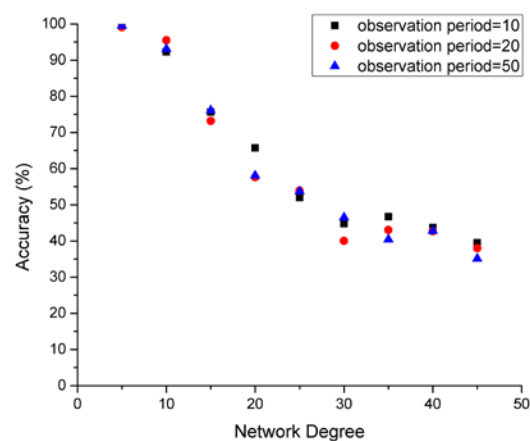


Figure 16. A comparison on the accuracy of early warning signal detection for different observation periods. A plot on the accuracy of early warning indicators (Moran coefficient spatial correlation) for 3 different observation periods versus the network degree. Note that each point is obtained after determining the percentage of significant accurate predictions through a comparison made against the null model.

5. Conclusion

We have investigated into the influence of complex social network interactions on regime shifts in coupled socio-ecological system as well as our ability to make accurate prediction on its occurrence. We have based our study using the TSL model, with the inclusion of social interactions modelled by different network topologies and employing a discrete choice mechanism to update agent's strategy which involves selection (utility driven strategy selection) and mutation (random strategy updating). Our results show that intrinsic social network properties can yield interesting multi-stable hysteresis structures, and can also have subtle effects on the accuracy of early warning signals. Thus, a more detailed understanding on the social interaction network properties as well as the associated socio-ecological parameters within a society would provide deeper insights that will be important for its proper protection. More importantly, it will enable us to improve our abilities to anticipate or even avoid the unsought for regime shift that can be catastrophic. In consequence, we perceive that the results of this work would be especially relevant and beneficial for decision making and management planning within the field of coupled socio-ecological systems.

References

1. Hoekstra, A. Y. Water scarcity challenges to business. *Nat. Clim. Change* **4**, 318–320 (2014).
2. Jarvis, A. J., Leedal, D. T. & Hewitt, C. N. Climate-society feedbacks and the avoidance of dangerous climate change. *Nat. Clim. Change* **2**, 668–671 (2012).
3. Parmesan, C. & Yohe, G. A globally coherent fingerprint of climate change impacts across natural systems. *Nature* **421**, 37–42 (2003).
4. Rosenberg, D. M., McCully, P. & Pringle, C. M. Global-Scale Environmental Effects of Hydrological Alterations: Introduction. *BioScience* **50**, 746–751 (2000).

5. Blank, L. W. West German forests: Deterioration, but some recovery. *Nature* **319**, 529–529 (1986).
6. Miller, G. H. *et al.* Ecosystem collapse in Pleistocene Australia and a human role in megafaunal extinction. *Science* **309**, 287–290 (2005).
7. Yasouri, M. Ecological limitations and sustainable regional development in khorassan province. *WSEAS Trans. Environ. Dev.* **5**, 126–135 (2009).
8. Jucan, C. & Jucan, M. Social Responsibility in Tourism and Sustainable Development. *WSEAS Trans. Environ. Dev.* **6**, 677–686 (2010).
9. Steffen, W., Crutzen, P. J. & McNeill, J. R. The Anthropocene: Are Humans Now Overwhelming the Great Forces of Nature. *AMBIO J. Hum. Environ.* **36**, 614–621 (2007).
10. Scheffer, M., Carpenter, S., Foley, J. A., Folke, C. & Walker, B. Catastrophic shifts in ecosystems. *Nature* **413**, 591–596 (2001).
11. Dent, C. L., Cumming, G. S. & Carpenter, S. R. Multiple states in river and lake ecosystems. *Philos. Trans. R. Soc. Lond. B. Biol. Sci.* **357**, 635–645 (2002).
12. Scheffer, M. & Carpenter, S. R. Catastrophic regime shifts in ecosystems: linking theory to observation. *Trends Ecol. Evol.* **18**, 648–656 (2003).
13. Scheffer, M. *et al.* Anticipating Critical Transitions. *Science* **338**, 344–348 (2012).
14. Nowak, M. A. & May, R. M. Evolutionary games and spatial chaos. *Nature* **359**, 826–829 (1992).
15. Lieberman, E., Hauert, C. & Nowak, M. A. Evolutionary dynamics on graphs. *Nature* **433**, 312–316 (2005).
16. Ohtsuki, H., Hauert, C., Lieberman, E. & Nowak, M. A. A simple rule for the evolution of cooperation on graphs and social networks. *Nature* **441**, 502–505 (2006).
17. Nowak, M. A., Tarnita, C. E. & Antal, T. Evolutionary dynamics in structured populations. *Philos. Trans. R. Soc. B Biol. Sci.* **365**, 19–30 (2010).
18. Palla, G., Derényi, I., Farkas, I. & Vicsek, T. Uncovering the overlapping community structure of complex networks in nature and society. *Nature* **435**, 814–818 (2005).
19. Weng, L., Menczer, F. & Ahn, Y.-Y. Virality Prediction and Community Structure in Social Networks. *Sci. Rep.* **3**, (2013).
20. Scheffer, M. Complex systems: Foreseeing tipping points. *Nature* **467**, 411–412 (2010).
21. Scheffer, M. *et al.* Early-warning signals for critical transitions. *Nature* **461**, 53–59 (2009).
22. Dakos, V. *et al.* Methods for Detecting Early Warnings of Critical Transitions in Time Series Illustrated Using Simulated Ecological Data. *PLoS ONE* **7**, e41010 (2012).
23. Dakos, V., van Nes, E. H., D’Odorico, P. & Scheffer, M. Robustness of variance and autocorrelation as indicators of critical slowing down. *Ecology* **93**, 264–271 (2012).
24. Dakos, V., Nes, E. H. van & Scheffer, M. Flickering as an early warning signal. *Theor. Ecol.* **6**, 309–317 (2013).
25. Dakos, V., Nes, E. H. van, Donangelo, R., Fort, H. & Scheffer, M. Spatial correlation as leading indicator of catastrophic shifts. *Theor. Ecol.* **3**, 163–174 (2009).
26. Livina, V. N. & Lenton, T. M. A modified method for detecting incipient bifurcations in a dynamical system. *Geophys. Res. Lett.* **34**, L03712 (2007).
27. Carpenter, S. R. & Brock, W. A. Rising variance: a leading indicator of ecological transition. *Ecol. Lett.* **9**, 311–318 (2006).
28. Seekell, D. A., Carpenter, Stephen R. & Pace, M. L. Conditional Heteroscedasticity as a Leading Indicator of Ecological Regime Shifts. *Am. Nat.* **178**, 442–451 (2011).
29. Held, H. & Kleinen, T. Detection of climate system bifurcations by degenerate fingerprinting. *Geophys. Res. Lett.* **31**, L23207 (2004).
30. Biggs, R., Carpenter, S. R. & Brock, W. A. Turning back from the brink: detecting an impending regime shift in time to avert it. *Proc. Natl. Acad. Sci. U. S. A.* **106**, 826–831 (2009).
31. Hastings, A. & Wysham, D. B. Regime shifts in ecological systems can occur with no warning. *Ecol. Lett.* **13**, 464–472 (2010).
32. Boettiger, C. & Hastings, A. Early warning signals and the prosecutor’s fallacy. *Proc. R. Soc. Lond. B Biol. Sci.* **279**, 4734–4739 (2012).
33. Boettiger, C. & Hastings, A. Quantifying limits to detection of early warning for critical transitions. *J. R. Soc. Interface* rsif20120125 (2012).
34. Hardin, G. The Tragedy of the Commons. *Science* **162**, 1243–1248 (1968).
35. Toba, D., Simion, D., Vochita, L. & Toba, E. Natural Dimension of Sustainable Development and Economic and Ecological Integration in the Evaluation of Social Welfare. *WSEAS Trans. Environ. Dev.* **7**, 13–22 (2011).
36. Sethi, R. & Somanathan, E. The Evolution of Social Norms in Common Property Resource Use. *Am. Econ. Rev.* **86**, 766–88 (1996).
37. Noailly, J., Withagen, C. A. & Bergh, J. C. J. M. van den. Spatial Evolution of Social Norms in a Common-Pool Resource Game. *Environ. Resour. Econ.* **36**, 113–141 (2007).
38. Tavoni, A., Schlüter, M. & Levin, S. The survival of the conformist: social pressure and renewable resource management. *J. Theor. Biol.* **299**, 152–161 (2012).
39. Carl Boettiger, A. H. No early warning signals for stochastic transitions: insights from large deviation theory. *Proc. Biol. Sci.* **280**, 20131372 (2013).
40. Kéfi, S. *et al.* Early Warning Signals of Ecological Transitions: Methods for Spatial Patterns. *PLoS ONE* **9**, e92097 (2014).
41. Okabe, A. & Sugihara, K. in *Spatial Analysis along Networks* 137–151 (John Wiley & Sons, Ltd, 2012).
42. Chung, F. & Lu, L. Connected Components in Random Graphs with Given Expected Degree Sequences. *Ann. Comb.* **6**, 125–145 (2002).
43. Lancichinetti, A., Fortunato, S. & Radicchi, F. Benchmark graphs for testing community detection algorithms. *Phys. Rev. E* **78**, 046110 (2008).

Appendix: Analytical Approximation

The solution of resource equilibrium is $\frac{\Delta R}{\Delta t} = 0$

$$R^* = \left(-E + \sqrt{E^2 + 4c \frac{d}{R_{max}}} \right) \frac{R_{max}^2}{2d}$$

Suppose there are 2 communities only. Let $P(D_1)$ be the probability that a defector from community 1 is selected to update its strategy while $P(C_1|D_1)$ is the probability that a defector from community 1 compares his payoff with a neighbouring co-operator from community 1. Since the probability of a defector changing its strategy to a co-operator depends on its utility comparison $[U_c - U_d]/U_c$ and probability that a defector is mutating is $1/m_p$. Moreover, the fraction of a node is connected with their own community is μ and fraction of a node is connected with other community is $1 - \mu$. Then by considering updating possibility from both communities, the probability that the total number of co-operator would increase by one is given by:

$$T^+(N_c) =$$

$$P(D_1) \left((1 - \mu)P(C_1|D_1) + \mu P(C_2|D_1) \right) \frac{u_c - u_d}{u_c} + P(D_1) \frac{1}{m_p} + P(D_2) \left((1 - \mu)P(C_2|D_1) + \mu P(C_1|D_2) \right) \frac{u_c - u_d}{u_c} + P(D_2) \frac{1}{m_p}$$

Similarly, the probability that the number of co-operator would decrease by one is given as follow:

$$T^-(N_c) =$$

$$P(C_1)\left((1-\mu)P(D_1|C_1) + \mu P(D_2|C_1)\right)\frac{u_d - u_c}{u_d} + P(C_1)\frac{1}{m_p} + P(C_2)\left((1-\mu)P(D_2|C_1) + \mu P(D_1|C_2)\right)\frac{u_d - u_c}{u_d} + P(C_2)\frac{1}{m_p}$$

We then construct the following master equation:

$$P\left(f_c, t + \frac{1}{N}\right) - P(f_c, t) = P\left(f_c - \frac{1}{N}, t\right)T^+\left(f_c - \frac{1}{N}\right) - P(f_c)T^-(f_c) + P\left(f_c + \frac{1}{N}\right)T^-\left(f_c + \frac{1}{N}\right) - P(f_c)T^+(f_c)$$

By expanding the master equation using Taylor series in $1/N$ and neglect the higher order terms, we may approximate differential equation of the strategy dynamics

$$\frac{d}{dt}P(f_c, t) = -\frac{d}{df_c}\left[P(f_c, t)(T^+(f_c) - T^-(f_c))\right]$$

The condition of social equilibrium is $T^+(f_c) - T^-(f_c) = 0$. In the case when mutation is rare, we can approximate $\frac{1}{m_p} \cong 0$ and drop the mutation term. Furthermore, by using the probability identity: $P(C)P(D|C) = P(D)P(C|D) = P(CD)$, we can rewrite the previous equation in the following form:

$$[(P(C_1D_1) + P(C_2D_2))(1-\mu) + (P(C_1D_2) + P(C_2D_1))\mu][U_c - U_d] = 0$$

With $U_c > 0$ and $U_d > 0$, the above equation can be written in the following form:

$$\sum_{i,j} [(P(C_1D_1)P(D_1) + P(C_2D_2)P(D_2))(1-\mu) + (P(C_1D_2)P(D_2) + P(C_2D_1)P(D_1))\mu](O(i+j) - \pi_d(f_c)) = 0$$

To solve this equation, we assume the co-operators and defectors are connected randomly. Let i be the number of neighbouring co-operators from own community and j be the number of neighbouring co-operators from other community. Since the total links of a node from own community is $k_c = k(1-\mu)$ and the total links of a node from the other community $k_{nc} = k\mu$, by using this random assumption, we can write the probability distributions of co-operators neighbours of a particular defector:

$$P(C_1|D_1) = \binom{k_c}{i} (C_1)^i (1-C_1)^{k_c-i} \binom{k_{nc}}{j} (C_2)^j (1-C_2)^{k_{nc}-j}$$

$$P(C_2|D_1) = \binom{k_{nc}}{j} (C_2)^j (1-C_2)^{k_{nc}-j} \binom{k_c}{i} (C_1)^i (1-C_1)^{k_c-i}$$

$$P(C_1|D_2) = \binom{k_{nc}}{j} (C_1)^j (1-C_1)^{k_{nc}-j} \binom{k_c}{i} (C_2)^i (1-C_2)^{k_c-i}$$

$$P(C_2|D_2) = \binom{k_c}{i} (C_2)^i (1-C_2)^{k_c-i} \binom{k_{nc}}{j} (C_1)^j (1-C_1)^{k_{nc}-j}$$

From the numerical result, we can infer that the cooperation/ defection spread in one community first before spread to other community. Therefore, let assume $C_1 = 2f_c$ and $C_2 = 0$ if $f_c < 0.5$. Similarly, let assume $C_1 = 1$ and $C_2 = 2f_c - 1$ if $f_c > 0.5$.

We then plot in figure A the set of stable and unstable fixed points as a function of the control parameter c for $k=15$ and $k=45$. The solid line represents the set of stable fixed points and the dashed line represents the set of unstable fixed points. Regime shift occurs at the point where the stable and unstable fixed points intersect which is associated with fold bifurcation. Our analytical estimation affirms the existence of multiple stable states. However due to the limitation of our assumption the analytical result and numerical result do not match perfectly. To obtain better analytical result we need to improve our assumption especially the connection distribution between co-operators and defectors and the spreading pattern of co-operators or defectors from one community to the others

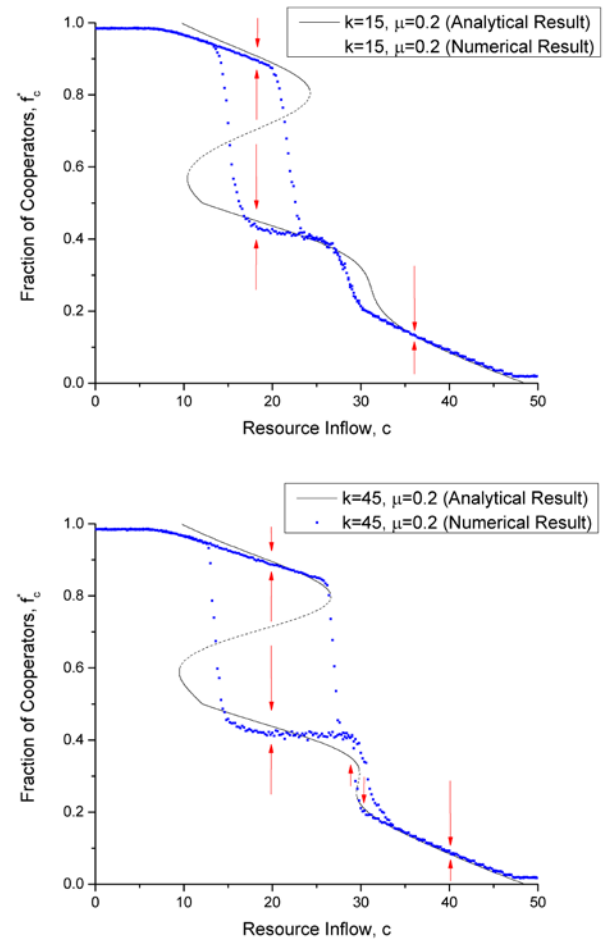


Figure A. Comparison between the analytical results and the numerical results for the case of (a) $k=15$ and (b) $k=45$ with strong community structures ($\mu = 0.2$). Note that the numerical result is represented as square. The solid line represents the set of stable fixed points and the dashed line represents the set of unstable fixed points.